Coordination of five class III peroxidase encoding genes for early germination events of Arabidopsis thaliana

Achraf M Jemmat, Philippe Ranocha, Aurélie Le Ru, Maxime Neel, Alain Jauneau, Sara Raggi, Simone Ferrari, Vincent Burlat, Christophe Dunand

Coordination of five class III peroxidase encoding genes for early germination events of *Arabidopsis thaliana*.

Achraf M Jemmat[1,a,†], Philippe Ranocha[1,†], Aurélie Le Ru[2], Maxime Neel[1], Alain Jauneau[2], Sara Raggi[3,b], Simone Ferrari[c], Vincent Burlat[a,*], Christophe Dunand[a,*]

[1] Université de Toulouse, UPS, UMR 5546, Laboratoire de Recherche en Sciences Végétales, BP 42617, F-31326 Castanet-Tolosan, France.

[2] Fédération de Recherche 3450, Plateforme Imagerie, Pôle de Biotechnologie Végétale, Castanet-Tolosan 31326, France.

[3] Institute Pasteur-Fondazione Cenci Bolognetti and Dipartimento di Biologia e Biotecnologie "Charles Darwin", Sapienza Università di Roma, 00185 Rome, Italy

[†] co-first authors

[a] Present address: Institute for Botany and Molecular Genetics, BioEconomy Science Center, Worringer Weg 3, RWTH Aachen University, Aachen 52074, Germany. [b] Present address: Umeå Plant Science Centre, Department of Forest Genetics and Plant Physiology, Swedish University of Agricultural Sciences, SE-901 83 Umeå, Sweden

[*] correspondence: burlat@lrsv.ups-tlse.fr, dunand@lrsv.ups-tlse.fr, +33 (0)5 34 32 38 58

e-mail address for each author

Achraf M Jemmat, Jemmat@bio1.rwth-aachen.de

Philippe Ranocha, ranocha@lrsv.ups-tlse.fr

Aurélie Le Ru, leru@lrsv.ups-tlse.fr

Maxime Neel, maxime.neel@hotmail.fr

Sara Raggi, sara.raggi@slu.se

Simone Ferrari, simone.ferrari@uniroma1.it

Coordination of five class III peroxidase encoding genes for early germination events of *Arabidopsis thaliana*.

Five Class III peroxidases have specific spatio-temporal expression pattern and antagonistic effects to control the endosperm cell wall rupture during Arabidopsis seed germination events

Abstract (236 words)

The Class III peroxidases (CIII Prxs) belong to a plant-specific multigene family. Thanks to their double catalytic cycle they can oxidize compounds or release reactive oxygen species (ROS). They are either involved in different cell wall stiffening processes such as lignification and suberization, in cell wall loosening or defense mechanisms. Germination is an important developmental stage requiring specific peroxidase activity. However, little is known about which isoforms are involved. Five CIII Prx encoding genes: *AtPrx04*, *AtPrx16*, *AtPrx62*, *AtPrx69*, and *AtPrx71* were identified from published microarray data mining. Delayed or induced testa and endosperm rupture were observed for the corresponding CIII Prx mutant lines indicating either a gene-specific inducing or repressing role during germination, respectively. Via *in situ* hybridization *AtPrx16*, *AtPrx62*, *AtPrx69* and *AtPrx71* transcripts were exclusively localized to the micropylar endosperm facing the radicle, and transcriptomic data analysis enabled positioning the five CIII Prxs in a co-expression network enriched in germination, cell wall, cell wall proteins and xyloglucan hits. Evidence were produced showing that the five CIII Prxs were cell wall-targeted proteins and that the micropylar endosperm displayed complex cell wall domain topochemistry. Finally, we drew a spatio-temporal model highlighting the fine sequential gene expression and the possible involvement of micropylar endosperm, cell wall domains to explain the non-redundant cell wall stiffening and loosening functions of the CIII Prxs in a single cell type. We also highlighted the necessity of a peroxidase homeostasis to accurately control the micropylar endosperm cell wall dynamics during Arabidopsis germination events.

Key words: Arabidopsis, Class III peroxidase, testa rupture, micropylar endosperm rupture, germination, cell wall domain remodeling,

Abbreviations: Class III peroxidase (CIII Prx), micropylar endosperm (MEN), reactive oxygen species (ROS).

Introduction

Seeds are important resistant structures because they ensure the transition between two successive generations. *Arabidopsis thaliana* mature seed formation takes about twenty days and seeds are composed of three main tissues: (i) the testa or seed coat, (ii) the endosperm which is divided into 3 parts (the peripheral, the chalazal and the micropylar endosperm, the latter being adjacent to the radicle) and (iii) the embryo which is enclosed in the first two compartments (Dekkers et al., 2013).

Germination is the focus of numerous studies since it represents a crucial process by which the embryo will start to grow in order to develop a seedling. It starts after imbibition and resuming of the metabolic activity. Germination is considered as completed when root, hypocotyl, and cotyledons can be observed. *Sensu stricto* germination ended with the embryo emergence (usually the radicle first) and consists in two observable events: the testa rupture (TR) due to the embryo and endosperm expansion and the (micropylar) endosperm rupture (ER) {Dekkers, 2013; Lariguet, 2013; Nonogaki, 2007}. Several aspects of this agro-economically relevant developmental stage have been previously analyzed in details. Beside the well-known hormonal balance control of germination by the antagonist ABA and GA_3 phytohormones (Ali-Rachedi et al., 2004; Penfield and Hall, 2009), we started to have a knowledge about micropylar endosperm cell wall proteins influencing this process by facilitating the TR and the ER. As examples, genes encoding endo-β-mannanase isoforms (MAN) (Iglesias-Fernández et al., 2011) or a pectin methylesterase inhibitor (PMEI5/At2g31430) {Müller, 2013} have been characterized.

Reactive oxygen species (ROS) initially described as cell-damaging by-products, can also be produced in a controlled manner for a specific purpose. In particular, embryo releases ROS through the seed coat to protect the emerging embryo against pathogen attacks {Schopfer, 2001}. They have also a function during seed germination and dormancy break {Ogawa, 2001; Müller, 2009, Barba-espin, 2010, Leymarie, 2012}. Among the battery of proteins able to regulate ROS homeostasis, NADPH oxidases, class III peroxidases (CIII Prx), and thioredoxins have a role during germination {Müller, 2009; Ortiz-Espín, 2017; Lariguet, 2013; Linkies, 2010}.

Peroxidase enzymes catalyze the oxidation of substrate to the detriment of hydrogen peroxide (Francoz et al., 2014). CIII Prxs are exclusive of the green lineage and have a broad range of functions like for example, auxin catabolism, lignin polymerization, cell wall domain loosening or defense responses (Cosio and Dunand, 2009; Francoz et al., 2014; 2019a; Hiner et al., 2002; Passardi et al., 2005). They constitute a multigenic family in plants and are mainly considered as secreted proteins: 73 members have been identified in *A. thaliana* (Tognolli *et al.*, 2002), and

thanks to their dual peroxidative and hydroxylic cycle, they contribute to the cell wall stiffening by the radical coupling of aromatic compounds and to cell wall loosening by the non-enzymatic polysaccharide breaking thank to ROS production, respectively (Passardi et al., 2005). Due to the high sequence conservation of CIII Prxs within species, putative functional redundancy is expected which explains the difficulty to attribute a specific function to each member of this large multigenic family (Cosio and Dunand, 2009). Several recent studies illustrated both this possible functional redundancy and conversely the means by which individual CIII Prxs may reach their specificity. The elegant demonstration of the involvement of a lignin molecular brace controlling the abscission of sepals and petals from the receptacle showed that 23 out of the 73 *CIII Prxs* were differentially expressed between the receptacle and the secession cells, impairing the identification of individual *CIII Prx* mutants with abscission phenotype (Lee *et al.*, 2018). Similarly, in search of the CIII Prx involved in Casparian strip lignification in the root endodermis, the quadruple mutant *atprx3/9/39/72* for four co-expressed *AtPrxs* did not display a Casparian strip lignification phenotype arguing for possible functional redundancy (Lee *et al.*, 2013). However, in the same study, AtPrx64, a fifth co-expressed CIII Prx was demonstrated to be anchored by the help of the trans-membrane CASP1 protein in the Casparian strip cell wall domain, enabling the lignification of the Casparian strip in the root endodermis (Hosmani et al., 2013; Lee et al., 2013). Moreover, AtPrx36 which is specifically produced in the outermost integument cells (oi2) during the seed development at torpedo stage and localized at the junction of radial/outer periclinal cell wall microdomain of the seed coat, is involved in the mucilage extrusion by controlling the polarized oi2 cell wall domain loosening (Kunieda et al., 2013; Francoz et al., 2019a). Therefore, CIII Prxs commonly appear as functionally redundant and rare recent examples start making a link between the specific activity of individual members because of spatio-temporal positioning to remodel cell wall domain zones. The molecular mechanisms enabling such accurate positioning of individual CIII Prxs in cell wall domains start to be uncovered (Hosmani et al., 2013; Lee et al., 2013; Francoz et al., 2019a). However, to date there are no studies showing within a single cell type, the localization of individual CIII Prxs in multiple cell wall domains and/or individual cell wall domain microphenotype of the corresponding mutants.

In addition, CIII Prxs are also able to regulate ROS homeostasis (Cosio and Dunand, 2009) to protect the embryo emergence against pathogens (Schopfer et al., 2001) or to control cell wall loosening or stiffening thus leading to a probable TR an ER boosting or delay, respectively. A *Lepidium sativum* transcriptomic search led to the demonstration of a germination acceleration phenotype in *atprx16* mutant from *A. thaliana* (Linkies *et al.*, 2010). Here, using recently published tissue-specific transcriptomics focused on *A. thaliana* germination (Dekkers *et al.*, 2013), we

identified a micropylar and chalazal endosperm-specific co-expression cluster encompassing five *CIII Prxs* including *AtPrx16*. We showed that the expression was restricted to the micropylar endosperm and that the corresponding proteins were localized to the cell wall. We also showed either a delayed or accelerated germination phenotype for each corresponding individual mutant ruling out the possibility of functional redundancy. In depth analysis of these expression cluster enabled us identifying enrichment in cell wall, cell wall protein and xyloglucan hits. We also produced a comprehensive topochemical characterization of micropylar endosperm cell walls showing a complex multi-cell wall domain organization. Finally, we discuss how sequential temporal gene expression and cell wall domains could account for the implication of CW remodeling enzymes from multigenic families, including *CIII Prxs*, to control micropylar endosperm cell wall dynamics during seed germination.

Materials and methods

Microarray data analysis and expression clustering of *Class III peroxidases*

All *CIII Prx* expression values were retrieved in a Microsoft Excel file from the microarray data deposited by (Dekkers *et al.*, 2013) in the national center for biotechnology information Gene expression Omnibus with accession number GSE 41212 (ww.ncbi.nlm.nih.gov/geo/). The raw data was first annotated and edited by sorting the genes according to their maximal log2 expression value and by identifiying the genes whose expression values were above the cutoff log2 value of "5" previously defined (Dekkers *et al.*, 2013). The generated Microsoft Excel file was then analyzed by different means. (i) *AtPrx62* which was the earliest *CIII Prx* to be higly expressed in the Micropylar and chalazal endosperm (MCE) pool, was chosen as a bait to calculate the Pearson Correlation Coefficient (PCC) along with all the genes of the data array. The genes were sorted and ranked following decreasing PCC values. Only the *CIII Prxs* were selected and their relative ranking and PCC were displayed alowing to select five MCE-sequentially expressed *CIII Prx* candidates. The expression profiles were highlighted with a red (maximal value)-to-yellow (cutoff 5)-to grey (values below the cutoff) heat map. (ii) The co-expression networks of the five selected *CIII Prxs* were similarly built and the four other *CIII Prxs* were positioned in each of the network to identify the *AtPrx69* network as those displaying the best co-expression of the five *CIII Prxs*. (iii) The AtPrx69 network was analyzed in depth using 12 lists of genes consituting so-called "tool boxes" related to subcellular compartments, cell wall polymers and physiological processes. The

the search tool from TAIR (https://www.arabidopsis.org/index.jsp). Each tool box was used to search and filter the corresponding hits within the *AtPrx69* network. For each hit, the relative rank (%) was calculated by dividing the "tool box rank" by the "absolute rank. Results were sumarrized by plotting the relative rank (y axis) *vs.* the PCC (x axis) for each of the cross-analysis.

Plant material and seed germination assays

Wild type Col-0 *A. thaliana* (Col) and T-DNA insertions lines in Col background (*atprx04-1* [SALK_110617], *atprx04-3* [FLAG_242H09], *atprx16-1* [SAIL_317_H04], *atprx16-2* [SALK_118245], *atprx62-1* [GK_287E07], *atprx62-2* [SALK_151762], *atprx69-1* [SAIL_691_G12], *atprx69-2* [SALK_137991], *atprx71-1* [SALK_123643] and *atprx71-2* [SALK_121202]) were obtained from the European Arabidopsis Stock Centre (http://arabidopsis.info/) and the INRA Versailles Stock Centre (http://publiclines.versailles.inra.fr). Using standard procedures, homozygous mutant plants were identified by PCR genotyping with respective primers (Table S16). T-DNA insertion sites were confirmed by sequencing using the same primers.

Seeds of the Col and mutant lines were simultaneously grown in Jiffy peat pellets under the same conditions (continuous light, 120 µmol photons.m^{-1}.s^{-1}, 22°C, 67 % relative humidity) in order to obtain homogeneous seed batches. For *in vitro* experiments, seeds were surface-sterilized with a solution containing 30 % bleach (v/v), 0.1 % triton X-100 (v/v), Seeds were put by spots of 50 to 100 seeds in Petri dishes containing ½ MS medium including sucrose (10 g.L^{-1}) with or without 200 mM NaCl for stress conditions. Petri dishes were stored at 4°C for cold stratification during 24-48 hours, and incubated in a germination cabinet with continuous light (77 µmol photons.m^{-1}.s^{-1}, 24°C) for the germination time course.

At different points of the germination kinetics (18, 24, 30, 32, 36, 38, 44, 50 and 77 hours after sowing (HAS) for Col, *atprx04-1* and *atprx16-1* and 24 and 36 HAS for at least 4 repeats with all the lines from 200 seed per batches), the Petri dishes were observed using a Zeiss Axiozoom V16 stereomicroscope. The seed pictures were analyzed using ImageJ to categorize and count the seeds at different germination stages: 1- intact testa and endosperm, 2- the testa rupture (TR) and 3- the endosperm rupture (ER).

***In situ* hybridization**

in situ RNA hybridization was realized essentially as previously described (Francoz et al.,

[http://www.brc.riken.jp/lab/epd/catalog/cdnaclone.html; (Seki et al., 1998, Seki et al., 2002)] as templates : *AtPrx16* (pda18344), *AtPrx62* (pda13156), *AtPrx69* (pda07505), *AtPrx71* (pda06662). *AtPrx04* cDNA was directly cloned in pGEMT-easy using the primers prx04_S-rt and prx04CodSequ-SmaI/AS listed in Table S16. Hundreds of Col seeds at various developmental stages were fixed in FAA, infiltrated in paraplast and allowed to sediment in 50 ml falcon tubes used as primary embedding molds. Following paraplast solidification at 4°C, each samples of the kinetics were unmolded, and the resulting paraplast blocks were trimmed and assembled in a final metallic embedding mold constituting a tissue microarray encompassing hundreds of seeds from each developmental stage. Serial sections were deparaffinized and used for the previously described *in situ* hybridization protocol (Francoz et al., 2016a; Francoz et al., 2019b). Slides were then scanned using the Nanozoomer 2.0HT (Hamamatsu Photonics, Tokyo, Japan). After scanning the image analysis was performed using the Hamamatsu photonics, Image viewer (NanoZoomer Digital Pathology, NDP) for "Virtual Microscopy". To insure fair comparison, the same individual seeds hybridized with the 10 riboprobes were retrieved on the synchronized scans from the serial sections and used for Fig. mounting and semi-quantitative analysis of signal intensities.

Transient expression in *Nicotiana benthamiana* leaves

AtPrx04, AtPrx16, AtPrx62, AtPrx69 and AtPrx71 coding sequences were amplified by PCR using cDNAs from *A. thaliana* 10-day old plantlets with the primers listed in Table S16. The PCR products were digested with the appropriate restriction enzymes and cloned into TagRFP-AS-N vector (Evrogen).

AtPrx04, AtPrx16, AtPrx62, AtPrx69 and AtPrx71-TagRFP fusions were subcloned (LR reaction, Gateway Technology, Invitrogen) into pEAQ-HT-DEST1 vector (Sainsbury *et al.*, 2009). Every construct was checked by restriction analysis and sequencing, and transferred into *Agrobacterium tumefaciens* (strain GV3101). The aquaporin PIP2A-YFP fusion protein pm-yb CD3-1006 (Nelson *et al.*, 2007) was used as a plasma membrane marker. Alternatively, the endoplasmic reticulum sp-YFP-HDEL (En Re) marker CD3-958 (Nelson *et al.*, 2007) was also used.

A. tumefaciens strains grown at an optical density of 0.5 at 600 nm and containing each Prx-TagRFP and PIP2A-YFP or sp-YFP-HDEL constructs were co-infiltrated using a ratio of ⅔ AtPrx-TagRFP – 1/3 into *N. benthamiana* 30-day old lower side leaves. 48 hours after infiltration, the leaves were detached, couterstained with Calcofluor and infiltrated or not in 30% glycerol for 5-10

sequential mode: Sequence 1 for Calcofluor (excitation: 405 nm ; emission 416-468 nm), sequence 2 for TagRFP (excitation: 561 nm; emission: 556-605 nm or excitation: 543 nm; emission: 555-636 nm); sequence 3 for YFP (excitation: 488 nm; emission: 498-559 nm). 1024x1024 images corresponded to single confocal sections merged and false colored using ImageJ (http://imagej.nih.gov/ij/).

RNA isolation and residual gene transcript analysis by end-point RT-PCR

Total RNA was prepared from 10-day old *in vitro*-grown Col and mutant plantlets using the Tri-reagent solution (Sigma-Aldrich). After quantification by spectrophotometry and verification by electrophoresis, RNA was treated with the RQ1 RNase-free DNase I (Promega) and quantified again. One microgram of total RNA was reverse transcribed using the oligo(dT)15 primer and the MMLV-RT (Promega) according to the manufacturer's instructions. PCR was carried out with the gene-specific intron-spanning primers (Table S16). The cycling conditions were 94°C for 3 min, followed by 94°C for 30 s, 60°C for 30 s and 72°C for 1 min, for 20 to 40 cycles. The PCR was ended with one final step at 72°C for 5 min, and analyzed by gel electrophoresis and ethidium bromide staining. The signal from the actin-encoding *ACT2* gene (Fulton and Cobbett, 2003) was used as a control for cDNA quantity and quality. Three independent experiments were performed with consistent results.

Peroxidase activity.

Soluble proteins were extracted from seeds 24 HAS grinded in 20mM HEPES, pH 7.0, containing 1 mM EGTA, 10mM ascorbic acid, and PVP PolyclarAT (100mg g^{-1} fresh material; Sigma). The extract was centrifuged twice for 10 min at 10,000 g. Each extract was assayed for protein levels with the Bio-Rad assay (Bio-Rad) and for total peroxidase activity following the oxidation of 8 mM guaiacol (Fluka) at 470 nm in the presence of 2 mM H_2O_2 (Carlo Erba) in a 200 mM phosphate buffer pH 6.0. Enzyme activity was expressed in nkatal/mg protein. Values are the mean of three replicates ± SD. P-value of one-way anova followed by Tukey's significance test, (**) $P < 0.001$, (***) $P < 0.0001$.

Immunofluorescence screening

Dry *A. thaliana* Col seeds were embedded in LR White resin using an optimized protocol adapted for this dry material (Francoz et al., 2019b). Semi-thin serial sections (1 µm) were disposed on silane coated microscopy slides and either stained with toluidine blue (TBO) or Calcofluor for

of 38 cell wall probes (http://www.plantprobes.net; Ralet et al., 2010) listed in Table S17: The secondary antibody was anti-Rat IgG-Alexa488, anti-mouse IgG-Alexa488 or anti-His-Alexa488 (Invitrogen) as detailled in Table S17. Attempts to perform a calcofluor couterstaining resulted in irregular efficiency of staining. The slides were then mounted in ProLong® Gold Antifade medium and imaged using confocal microscopy. HCX APO CS 63.0 x 1.40 oil immersion objective under sequential mode: Sequence 1 for Alexa488 (excitation: 488 nm; emission: 499-578 nm), sequence 2 for Calcofluor/autofluorescence (excitation: 405 nm ; emission 426-468 nm). Images corresponded to single confocal sections merged and false colored using ImageJ (http://imagej.nih.gov/ij/).

Phylogenetic analysis and taxonomic distribution

The 10 CIII Prx protein sequences including AtPrx69, AtPrx71, AtPrx16, AtPrx62, AtPrx04, their paralogs and AtPrx42 as outgroup sequence, were aligned using MAFFT. The tree was constructed using the Neighbor-Joining method (Saitou and Nei, 1987) and evolutionary analyses were conducted in MEGA7 with 100 bootstraps (Kumar *et al.*, 2016).

Taxonomic distribution of the four clusters along the green lineage was performed with OrthoMCL clustering. The numbers corresponded to the copy number found in each cluster.

All protein sequences used for phylogenetic analysis and taxonomic distribution are available from the PeroxiBase (http://peroxibase.toulouse.inra.fr, (Fawal *et al.*, 2013).

Results

Microarray analysis of *CIII Prx* expression profiles leads to a clusterized micropylar and chalazal endosperm specific pattern

In order to explore the role of CIII Prxs during seed germination, we extensively analysed published microarray dataset based on laser capture microdissection of different seed sections during the germination time course of *A. thaliana* (Dekkers *et al.*, 2013) (data are deposited in the NCBI gene expression omnibus, GSE 41212, and for complete list refer to Tables S1). Among the highly expressed *CIII Prxs* in the micropylar and chalazal endosperm (MCE) pool, *AtPrx62*, which was the earliest expressed *CIII Prx* during the studied kinetics, has been used as a bait to build a co-expression network ranked by decreasing individual Pearson correlation coefficient (PCC) among all this microarray dataset. Other CIII Prx-encoding genes were then selected based on their rank and PCC value (Fig. 1A; Tables S2). A MCE-specific *CIII Prx* cluster could be identified since four

additional *CIII Prxs* (*AtPrx69*, *AtPrx71*, *AtPrx16* and *AtPrx04*) were found within the 1,000 top genes belonging to the *AtPrx62* network with PCC values ranging from 0.888 to 0.739 and relatively high expression values (Fig. 1A; Tables S2). It should be noted that although these CIII Prxs are strongly expressed during the early germination steps with particular expression patterns, they have also been detected in other organs such as roots, stems and leaves {Shigeto, 2013; Arnaud, 2018}.

The expression of *AtPrx62* and *AtPrx69* sequentially started before the testa rupture (TR) and persisted until the completion of the endosperm rupture (ER). *AtPrx71*, *AtPrx16* and *AtPrx04* had a similar expression profile starting after the TR, slightly delayed as compared to *AtPrx62* and *AtPrx69*. Gene expression analysis using more global transcriptomic data overall confirmed the clusterization but with a lower level of resolution (Fig. 1B). *AtPrx62* was the earliest expressed gene among the five selected genes (expression from 3 h, Fig. 1A), and at 24 h and 48 h, the five selected genes were co-expressed. This co-expression was specific as compared to non-selected corresponding paralog genes for *AtPrx69*, *Atprx16* and *AtPrx04* (*AtPrx70*, *Atprx25* and *AtPrx05*, respectively). However, the low spatial resolution of global transcriptomic data (Fig. 1B), could lead to wrongly select *AtPrx46* as candidate while its expression is only restricted to cotyledons and radicle during germination but not to MCE (Fig. 1A). These results indicate the advantage of our approach in order to specifically select CIII Prxs involved in «seed germination». Considering the importance of both TR and ER events during the germination time course, and the availability of at least two independent T-DNA mutants for the five selected *CIII Prxs* (*AtPrx62, 69, 71, 16,* and *04*), we decided to perform cellular and sub-cellular localizations and phenotyping analysis.

***AtPrx62, AtPrx69, AtPrx71* and *AtPrx16* expression is restricted to the micropylar endosperm**

The tissue-specific transcriptomic study used here for the selection of the candidates was valuable since sampling was restricted to a limited number of tissues (Dekkers et al., 2013). However, the sampling of chalazal and micropylar endosperm pool could not discriminate whether the candidate genes were expressed within the micropylar endosperm (ME), the chalazal endosperm (CE), or both tissues. This piece of information was crucial to relate these genes to germination since the CIII Prx activity involved in seed germination is concentrated in the ME together with H_2O_2 (Lariguet *et al.*, 2013). As the complementarity between *in situ* hybridization (ISH) and transcriptomics has been demonstrated (Francoz *et al.*, 2016a), a systematic ISH experiment was engaged using digoxigenin-labelled riboprobes specific for each of the five *CIII Prx* candidate genes. Serial sections from the paraffin-embedded tissue array containing kinetics of hundreds of

germinating seeds around the time of TR and ER were used. Transcripts from *AtPrx62*, *AtPrx69*, *AtPrx71* and, to a lower extend, *AtPrx16* were specifically localized in the ME, and neither in the CE nor in the peripheral endosperm (PE), at 34 hour after sowing (HAS) (Fig. 2; Fig. S1 and S2). We carefully analyzed serial sections from individual seeds from the tissue microarray between 24 and 38 HAS with each riboprobe and summarized the semi-quantitative results (Fig. 3). The time window analyzed by ISH was compared to the transcriptomics kinetics (Fig. 3A, B). A relative coherence could be obtained between the transcriptomic expression levels and the ISH signal intensities, since *AtPrx69* displayed the best ISH signal while *AtPrx04* expression level was just below the ISH detection limit. Similarly, the correlation between transcriptomics and ISH was relatively good while looking at the kinetics since *AtPrx62* and *AtPrx69* were more readily detected than *AtPrx71* and *AtPrx16* at 26 HAS (Fig. 3A, B). Finally, this analysis at the individual-seed level through ISH performed on serial sections allowed monitoring the number of genes among the five *CIII Prxs* for which transcripts were simultaneously detected in the ME of a same seed (Fig. 3C). For example, at 34 HAS, transcripts from four out of the five *CIII Prxs* could be detected in the same seed for 23 % of the analyzed seeds. Beyond the MCE co-expression observed by transcriptomics, this semi-quantitative ISH results showed the actual co-expression restricted to the ME at the seed level of up to five *CIII Prxs*, raising the question of whether or not these genes had a redundant function in this tissue during germination.

AtPrx62, AtPrx69, AtPrx71 and AtPrx04 are cell wall-targeted class III peroxidases

In *A. thaliana*, 64 CIII Prxs are predicted or localized to the CW and 9 are targeted to the vacuole in relation with a C-terminal extension acting as a demonstrated or putative vacuolar targeting sequence (Carter *et al.*, 2004; Francoz *et al.*, 2015). Heterologous expression experiments were performed in *Nicotiana benthamiana* to assess whether these five CIII Prxs belonging to ME-specific expression cluster co-localized to the same subcellular compartment. Using constructs encoding for CIII Prx-TagRFP fusion proteins under the control of CaMV 35S promoter, transient expression experiments were conducted in *N. benthamiana* leaves with PIP2A-YFP used as a plasma membrane marker (Nelson et al., 2007) and Calcofluor as a CW marker. For three constructs (AtPrx62-TagRFP, AtPrx69-TagRFP and AtPrx71-TagRFP), we were able to detect a co-localization for the RFP, the YFP signals and the calcofluor CW counterstaining (Fig. 4). Under water mounting, the calcofluor signal (green false colored) co-localized with the RFP signal (magenta false colored) for the three constructs leading to a white signal when the two channels were merged, predicting a CW localization for AtPrx62, AtPrx69 and AtPrx71 (Fig. 4A-C). As

shown in Fig. 4D-L when the cells were plasmolyzed, the RFP signal was still localized to the cell wall while the YFP signal (green false colored) was essentially found in the plasma membrane, demonstrating that AtPrx62, AtPrx69 and AtPrx71 were targeted to the CW. This was in agreement with the fact that most of the CIII Prxs (including AtPrx62, AtPrx69 and AtPrx71) had a secretory pathway signal peptide. In addition, several studies have shown that CIII Prxs could have a function in the CW dynamics thanks to their CW loosening or stiffening roles (Francoz et al., 2015;. Wilson et al., 2015). AtPrx16-TagRFP fluorescence signal totally co-localized with signal peptide-YFP-HDEL used as an endoplasmic reticulum marker, respectively (Fig. S3A-C) while AtPrx04-TagRFP showed a cell wall localization with some residual retention to the endoplasmic reticulum (Fig. S3D-F). Therefore, although AtPrx04 and AtPrx16 both contained predicted secreted signal peptide and no C-terminal HDEL/KDEL endoplasmic reticulum retention signal, they seemed to be at least partially retained to the endoplasmic reticulum regardless of the time of observation following agroinfiltration. This surprising result was counterbalanced by the analysis of cell wall proteomics data (Fig. S3G) showing the detection of AtPrx04 and AtPrx16 in CW-enriched root fractions. AtPrx69,AtPrx71 and *Brassica olearacea* AtPrx62 ortholog were also detected in CW proteome in agreement with our confocal observations. Comparative analysis of subcellular proteomes confirmed the presence of these five CIII Prxs in CW-enriched fractions as compared to other sub-cellular compartment-enriched fractions, and did not show any detection of AtPrx04 and AtPrx16 in endoplasmic reticulum-enriched fractions (Fig. S3H). Altogether, AtPrx62, AtPrx69 and AtPrx71 are CW localized proteins and AtPrx04 and AtPrx16 are probably CW proteins as well. Therefore, these five CIII Prxs are good candidates to specifically or redundantly play a role in CW remodeling of the ME cells, thus accelerating or delaying the germination of *A. thaliana* seeds.

Class III peroxidases have antagonist effects on early germination steps

Two independent T-DNA mutant lines were isolated for each of the five genes (Fig. S4A). As demonstrated by RT-PCR, they were all knockout mutants except for *atprx04-1*, *atprx62-2* and *atprx71-2*, which presented 40-50 % residual transcriptional activity (Fig. S4A). Accordingly, significant reduction of the total peroxidase activity was observed in all mutant lines suggesting a relation between CIII Prx transcript and protein levels (Fig. S4C). Germination kinetics were performed and the three following stages were quantified: (i) intact testa and endosperm, (ii) testa rupture (TR) and (iii) endosperm rupture (ER) (Fig. 5A). Complete kinetics of germination were performed for wild-type seeds (Col) and two mutants that show opposite phenotypes (*atprx04-1* and *atprx16-1*) in order to determine the optimal time to well discriminate the two rupture events (Fig.

5B). Then, TR and ER rates were extensively assessed 24 hours after sowing (HAS) and 36 HAS, respectively. At 24 HAS, the TR was high enough and the ER more or less equal to zero to allow the observation of differences between all the different lines. In addition, at 36 HAS, the ER was also high enough and the TR close to 100 % to discriminate between the mutants.

At 24 HAS, *atprx04-1* and *atprx04-3* exhibited a severe TR delay (-75% and -52 % respectively) and *atprx16-1*, *atprx16-2*, *atprx69-1*, *atprx69-2*, *atprx71-1* and *atprx71-2* seeds showed a clear increase of TR (between 30% and 82%) when compared to the wild type (Fig. 5C). No significant effect was observed in *atprx62-1* and *atprx62-2* regarding the % of TR at 24 HAS. At 36 HAS, WT and mutants seeds had more than 80% of TR, which no longer allowed observing a significant TR phenotype (Fig. 5B). However, this second observation time revealed ER phenotypes. Indeed, *atprx04-1* and *atprx04-3* presented an ER delay (-44% and -63 % respectively, Fig. 5C) and the eight other mutants including the two *atprx62* lines presented a large increase of ER (between 58 to 206 %) as compared to the wild type seeds (Fig. 5D). Strikingly, despite the observed strong gene co-expression, mutants from all the five genes displayed a clear germination phenotype in disagreement with anticipated putative functional redundancy. To summarize, two opposite germination phenotypes were observed in the *CIII Prx* mutant lines: (i) TR and/or ER induction for *atprx16*, *atprx62*, *atprx69* and *atprx71* mutants suggesting a CW stiffening action of AtPrx16, AtPrx62, AtPrx69 and AtPrx71 that negatively regulates germination. (ii) TR and ER repression for the two a*tprx04* allelic mutants suggesting that AtPrx04 had a promoting CW loosening role on both testa and ME rupture. These phenotypes were observed for both KO and KD mutants suggesting that a 50-60% reduction of gene expression was sufficient to lose the function (Fig. 5C, D; Fig. S4B).

The process of germination is delayed in presence of salt concentration (Lee and Zhu, 2010) and public data indicate that the expression of *AtPrx04*, *AtPrx16*, *AtPrx62* and *AtPrx69* are regulated by salt stress at the seedling root level (Fig. S5A, {Killian, 2007}). The kinetics of TR and ER in presence of 200 mM NaCl were performed with Col, and two mutants with contrasted phenotypes (*atpr04-1* and *atprx16-1*, Fig. 5) and allowed determining the optimal reading frame of early germination steps (Fig. S5B). As expected, the TR and ER were both delayed and the germination rate was also reduced when Col seeds were grown with salt. In order to determine the putative relationship between salt and CIII Prx action, the TR was quantified 77 HAS for 5 mutants and compared with the results obtained without NaCl. For *atprx04-1*, the strong TR delay observed at 24 HAS without NaCl was no longer observed and converted to a slight TR induction at 77 HAS. For *atprx62-1* and *atprx16-1*, and to a lesser extent, for *atprx71-2*, seeds at 77 HAS in presence of NaCl showed a higher TR induction when compared with the germination performed without NaCl

(Fig. S5C). *atprx69-1* TR induction was slightly decreased in presence of NaCl. Therefore, mutants from *AtPrx04* and *AtPrx62* that were the most induced by salt treatment (Fig. S5A), were those displaying the most dramatical phenotype changes in presence of NaCl (attenuated and amplified phenotypes for *atprx04-1* and *atprx62-1*, respectively). These results suggested that among the five CIII Prxs, AtPrx62 seemed to be the most implicated in salt tolerance during germination. A link between salt stress tolerance during germination and CW remodeling has been recently proposed for a pectin methylesterase inhibitor (PMEI13/AT5G62360) and a pectin methylesterase (PME31/AT3G29090) since the germination phenotype of the corresponding mutants (overexpression and T-DNA respectively) were only revealed under salt stress conditions {Yan, 2018; Chen, 2018}.

The *CIII Prx* co-expression network is enriched in genes related to "germination", "cell wall" "cell wall proteins" and "xyloglucans".

In order to better understand the implication of the five CIII Prxs during early germination steps, each of the CIII Prx was used as a bait to generate five respective co-expression networks using the seed germination tissue-specific transcriptomics data (Dekkers et al. 2013). We compared the five networks in order to identify which one displayed the strongest co-expression of the five *CIII Prxs* (Tables S3A, B). *AtPrx69* co-expression network appeared as the most interesting to simultaneously analyze commonly co-expressed genes with the five *CIII Prxs*. We assembled twelve "tool box" lists of genes related to various sub-cellular compartments, cell wall components and physiological processes (Table S4B-15B), and used each of these tool boxes for a cross-comparison with *AtPrx69* co-expression network (Table S4A-15A). For each of these cross-analyses, we calculated the Pearson correlation coefficient and the relative rank corresponding to the ratio of the tool box rank *vs.* the initial absolute rank (see Methods for details). The results were summarized in 12 plots representing the relative rank (%) *vs.* the PCC for each of the tool box genes found in *AtPrx69* co-expression network, using the same x and y scales for fair comparison. It appeared that the *AtPrx69* co-expression network was clearly enriched in genes from the "cell wall" as compared to the other sub-cellular compartment tool boxes (Fig. 6A-D). The "cell wall genes" enrichment further supports the ME endosperm CW remodeling hypothesis. Interestingly, the comparison of tool boxes from different CW polymers revealed that *AtPrx69* co-expression network was enriched in "cell wall proteins" and in "xyloglucan" hits rather than in "cellulose" and "pectin" hits (Fig. 6E-H). This observation gave more insight on how the five CIII Prxs might regulate the ME CW dynamics through possible functional connections with these types of CW polymers.

Finally, while performing similar search using tool boxes related to different physiological processes, we observed the enrichment of *AtPrx69* co-expression network in hits from "seed germination" and not from "seed storage", "photosynthesis" and "cell division" used as controls (Fig. 6I-L). Altogether, these cross-analyses of transcriptomic data reinforced our experimental results indicating the role of the five CIII Prxs in ME CW dynamics controlling seed germination. These enrichments in categories of genes did not give direct evidence as to the role of the five CIII Prxs, but argued in favor of a potential ME CW modification function during seed germination in relation to xyloglucan. Bibliographic search within the "seed germination" hits from *AtPrx69* co-expression network showed that the best hits were the four other *CIII Prxs* coming from this study, as well as STEROL CARRIER PROTEIN 2, a unrelated peroxisomal protein involved in β-oxidation already described for its role during seed germination (Zheng *et al.*, 2008) (Table S12A). The other "germination hits" were found farther along the co-expression network indicating that the *CIII Prx* co-expression was somehow separated from the previously characterized genes for their role in germination suggesting that potential new candidates could be found between the position 270 and 2010 of the absolute rank.

Dry seed ME CW displayed topochemical specificities suggesting the occurrence of CW microdomains.

A previous immunofluorescence study illustrated the CW topochemistry of ME as compared to other seed tissues in *A. thaliana* imbibed seeds (Lee *et al.*, 2012). It appeared that ME CW was labeled with LM25 and to a lesser extent LM15 (xyloglucans), LM19 (unmethylesterified homogalacturonans), LM6, LM13 and LM16 (arabinans). Of particular interest was the different labeling observed with the arabinan-specific antibodies: LM13 labeled the inner and outer CW and not the radial CW while LM6 and LM16 labeled all the ME CW, illustrating the complexity and diversity of ME CW topochemistry. With the aim to better understand this complexity, we performed an additional systematic immunofluorescence screening focusing on serial longitudinal sections from dry seeds that are in the "starting blocks" preceding the action of the five studied CIII Prxs (Fig. 7; Fig. S17). We obtained ME-specific signals with 13 CW probes (Fig. 7). Interestingly, only LM25 and LM16 displayed an homogeneous labeling all around the ME CW (Fig. 7E, L). The remaining eleven probes all gave patchy and/or polarized and/or differentially intense labeling around ME CW (Fig. 7C, D, G, I-K, M-P, R). While Calcofluor cytochemical labeling of β-glucans including cellulose showed a regular labeling of ME walls, crystalline cellulose-specific labeling with CBM3a was restricted to the ME inner wall/radial wall corners (Fig. 7B, C). The LM15

labeling on ME inner wall and radial and outer wall patches contrasted with the LM25 more regular labeling (Fig.7D, E). LM15 recognizes somehow less substituted and shorter xyloglucan (XG) models than LM25, though the differences of specificity of these antibodies are subtle and complex (Pedersen et al., 2012; Ruprecht et al., 2017). The only homogalacturonan (HG) probe showing ME CW labeling was LM19 restricted to the inner wall (Fig. 7G). Four rhamnogalacturonan I (RGI) probes displayed labeling with a tendency of more intense labeling on the ME outer wall than on the inner wall and a patchy labeling pattern of RU2 (Fig. 7I-L). Contrarily, three extensin (EXT) antibodies show the somehow opposite pattern with regular labeling on the ME inner wall and less intense, absent or patchy labeling of the radial and/or outer wall (Fig. 7M-O). Finally, two arabino galactan protein (AGP) antibodies showed a patchy and/or polarized labeling (Fig. 7P-R). These results complemented those published on imbibed seeds (Lee *et al.*, 2012) since LM25 and LM16 gave similar ME CW labeling patterns in both studies while LM19, LM6, LM13 and JIM12 ME CW labeling patterns were more polarized in our study. The other antibodies were not presented in Lee et al (2012).This antibody panel and the previous study on imbibed seeds illustrated the complexity and diversity in the distribution of ME CW polymers since different topochemistries could be observed on the inner, radial and outer CW with some patchy labeling constituting multiple cell wall domains altogether suggesting the necessity for a correlated complexity/diversity in CW remodeling enzymes, in agreement with our results showing the involvement of five non redundant CIII Prxs in a single cell type.

In *A. thaliana*, AtPrx04, AtPrx16, AtPrx62, AtPrx69 and AtPrx71 belong to the same evolutionary cluster containing four other members (AtPrx05, AtPrx25, AtPrx45, AtPrx70). The five CIII Prxs selected in this study present from 34 to 74% identity (Fig. S6) All the genes member of this cluster were found to be expressed in roots and only the five selected genes presented a specific seed expression (Fig. S7A). The cluster resulted from four recent duplications in *A. thaliana* and also in other Brassicaceae (Fig. S7A and B, blue circles). Older duplications can be detected (Fig. S7A, orange circles) since no AtPrx04 and AtPrx69 orthologs has been detected before mono-/dicotyledon separation (Fig. S7B). From an evolutionary point of view, this raises questions on the putative neofunctionalization of some ortholog genes in Angiosperms, and on their possible conserved function in controlling germination.

Discussion

Germination is a critical stage during *A. thaliana* and other seed plants lifespan since it represents the transition between two successive generations (Salomé et al., 2008). This stage consists in two crucial and sequential events: the testa rupture and endosperm rupture necessitating CW remodeling, particularly in the ME facing the protruding radicle. Here, we exploited an elegant published microarray data (Dekkers et al., 2013) to identify a MCE co-expression cluster comprising five *CIII Prx* candidates (*AtPrx69, AtPrx71, AtPrx16, AtPrx62, AtPrx04).* We further demonstrated their expression in the ME rather than in the CE. This location is similar to that of the H_2O_2 that strongly accumulated in the distended endosperm prior its rupture (Lariguet *et al.*, 2013). We also provided evidence and discussion indicating that the five genes encoded CW proteins all displaying peroxidase activity. Interestingly, we observed a germination phenotype for the ten corresponding mutants in disagreement with the anticipated putative functional redundancy. Our results indicated that the ME remodeling was finely controlled by the coordinated action of four CIII Prxs (AtPrx62, 69, 71, 16) having a repressive role on TR and ER and one CIII Prx (AtPrx04) having the opposite activating role on TR and ER. The repressive role could be related with cell wall stiffening as suggested for AtPrx71 whose corresponding mutants display increased growth, enhanced leaf epidermal cell size (Raggi *et al.*, 2015) and lignin structure modification {Shigeto, 2013}. The activating role could be associated with cell wall loosening due to ROS spatio-temporal production as well as cell wall stiffening on the border of the rupture area. AtPrx04, which has been described to play a role in stem lignification {Fernandez, 2015}, could reinforce the cells around rupture region.

This raised the question on the means by which this coordination was achieved. Our ISH results demonstrated that at certain points of the kinetics, individual seeds actually co-expressed at least four of these genes. However, transcriptomics and ISH also demonstrated that the expression of these genes sequentially started at different time points. The four *CIII Prx* genes that were sequentially expressed at first were those encoding AtPrx62, 69, 71, 16 (Fig. 8A) suggesting a cumulative ME stiffening action of these enzymes that could counter-balance the increasing pressure of the growing radicle to avoid a premature germination (Fig. 8B). In turn, *AtPrx04* that encoded an enzyme that could account for the opposite ME CW loosening action was the last expressed among the five *CIII Prxs*, and its expression correlated with the ER (Fig. 8). The means by which these CIII Prxs either stiffened or loosened the ME CW is unknown but in depth cross-analysis of their co-expression network argued for a link with other CW proteins and possibly xyloglucans. Among the ME-expressed genes encoding CW remodeling or putative CW integrity sensors, members of three multigenic families were previously characterized. These corresponded to three mannanases (Iglesias-Fernandez *et al.*, 2011), three Lectin-receptor kinases (Xin *et al.*,

2009) and two xyloglucan xylosyltransferases (Lee *et al.*, 2012). One the one hand, single mutants of the three mananases displayed a germination delay phenotype similarly to the situation observed for the five CIII Prx mutants. On the other hand, clear germination phenotypes were observed with multiple mutants for the LecRKs and XXTs and never in single mutants. By comparing the ME-specific expression profiles of all these genes, it appeared that the non-redundant functions of the three MANs and the five CIII Prxs during ME CW remodeling was associated with a subtle sequential expression while the redundant functions of the three LecRKs and the two XXTs could be associated to more pronounced co-expression (Fig. 8A). It also appeared that the sequential expression of the three *MANs* preceded the sequential expression of of the four *CIII Prxs* that could account for stiffening action, together preceding the final expression of *AtPrx04* with putative loosening function (Fig. 8B). These combined results showed the complexity of ME CW remodeling allowing to finely tune the precise time of radicle protrusion. The particularity of CIII Prxs also relied on their involvement in both H_2O_2 cellular regulation and ROS generation which could have a role in CW dynamics through non enzymatic polysaccharide breaking or aromatic compounds covalent linking (Cosio and Dunand, 2009; Hiraga et al., 2001). However, the actual mode of action used by the five CIII Prxs to stiffen or loosen the ME CW still needs to be investigated. The precise localization of each of these enzymes within ME CW might be crucial for the developmental output as reported for two CIII Prxs localized in polarized CW microdomains in *Arabidopsis* seed coat or root endodermis (Kunieda *et al.*, 2013; Lee *et al.*, 2013; Francoz *et al.*, 2019a). So in addition to the subtle sequential temporal expression of the five *CIII Prxs*, we cannot exclude that putative localization of the corresponding proteins to ME CW domains could also account for the observed non redundant functions. This last hypothesis would fit with the observed ME CW topochemical heterogeneity.

Altogether, these results show that multiple CIII Prxs may have non redundant CW remodeling function in a given cell type in agreement with the emerging description of the localization of this type of enzyme to remote CW domains necessitating specific remodeling.

Acknowledgments

The authors are thankful to the Paul Sabatier Toulouse 3 University and to the *Centre National de la Recherche Scientifique* (CNRS) for granting their work. This work was also supported by the French Laboratory of Excellence project "TULIP" (ANR-10-LABX-41; ANR-11-IDEX-0002-02) and the French National Research Agency project ‘‘MicroWall’’ (ANR-18-CE20-0007). Thanks to Hinda Talaron and Jérémy Delpuech for their technical supports during the initial mutant screening and to Edith Francoz for resin embedding.

References

Carter C, Pan SQ, Zouhar J, Avila EL, Girke T, Raikhel NV. 2004. The vegetative vacuole proteorne of *Arabidopsis thaliana* reveals predicted and unexpected proteins. Plant Cell **16**, 3285-3303.

Cosio C, Ranocha P, Francoz E, Burlat V, Zheng Y, Perry SE, Ripoll JJ, Yanofsky M, Dunand C. 2017. The class III peroxidase PRX17 is a direct target of the MADS-box transcription factor AGAMOUS-LIKE15 (AGL15) and participates in lignified tissue formation. New Phytologist **213**, 250-263.

Dekkers BJW, Pearce S, van Bolderen-Veldkamp RP, Marshall A, Widera P, Gilbert J, Drost HG, Bassel GW, Muller K, King JR, Wood ATA, Grosse I, Quint M, Krasnogor N, Leubner-Metzger G, Holdsworth MJ, Bentsink L. 2013. Transcriptional dynamics of two seed compartments with opposing roles in Arabidopsis seed germination. Plant Physiology **163**, 205-215.

Fawal N, Li Q, Savelli B, Brette M, Passaia G, Fabre M, Mathé C, Dunand C. 2013. PeroxiBase: a database for large-scale evolutionary analysis of peroxidases. Nucleic Acids Res **41**, D441-444.

Francoz E, Ranocha P, Nguyen-Kim H, Jamet E, Burlat V, Dunand C. 2015. Roles of cell wall peroxidases in plant development. Phytochemistry **112**, 15-21.

Francoz E, Ranocha P, Pernot C, Le Ru A, Pacquit V, Dunand C, Burlat V. 2016a. Complementarity of medium-throughput in situ RNA hybridization and tissue-specific transcriptomics: case study of Arabidopsis seed development kinetics. Sci Rep **6**, 24644.

Francoz E, Ranocha P, Pernot C, Le Ru A, Pacquit V, Dunand C, Burlat V. 2016b. Complementarity of medium-throughput in situ RNA hybridization and tissue-specific transcriptomics: case study of Arabidopsis seed development kinetics. Scientific Reports **6**.

Francoz E, Ranocha P, Le Ru A, Martinez Y, Fourquaux I, Jauneau A, Dunand C, Burlat V. 2019a. Pectin demethylesterification generates platforms that anchor peroxidases to remodel plant cell wall domains. Dev Cell **48,** 261-276.

Francoz E, Ranocha P, Dunand C, Burlat V. 2019b. Medium-throughput RNA *in situ* hybridization of serial sections from paraffin-embedded tissue microarrays. Methods Mol Biol. **1933**, 99-130.**Fulton LM, Cobbett CS**. 2003. Two alpha-L-arabinofuranosidase genes in Arabidopsis thaliana are differentially expressed during vegetative growth and flower development. J Exp Bot **54**, 2467-2477.

Iglesias-Fernandez R, Rodriguez-Gacio MC, Barrero-Sicilia C, Carbonero P, Matilla A. 2011. Three endo-beta-mannanase genes expressed in the micropylar endosperm and in the radicle influence germination of *Arabidopsis thaliana* seeds. Planta **233**, 25-36.

Kumar S, Stecher G, Tamura K. 2016. MEGA7: Molecular Evolutionary Genetics Analysis Version 7.0 for Bigger Datasets. Mol Biol Evol **33**, 1870-1874.

Kunieda T, Shimada T, Kondo M, Nishimura M, Nishitani K, Hara-Nishimura I. 2013. Spatiotemporal secretion of PEROXIDASE36 is required for seed coat mucilage extrusion in Arabidopsis. Plant Cell **25**, 1355-1367.

Lariguet P, Ranocha P, De Meyer M, Barbier O, Penel C, Dunand C. 2013. Identification of a hydrogen peroxide signalling pathway in the control of light-dependent germination in Arabidopsis. Planta **238**, 381-395.

Lee BH, Zhu JK. 2010. Phenotypic analysis of Arabidopsis mutants: germination rate under salt/hormone-induced stress. Cold Spring Harb Protoc **2010**, pdb.prot4969.

Lee KJD, Dekkers BJW, Steinbrecher T, Walsh CT, Bacic A, Bentsink L, Leubner-Metzger G, Knox JP. 2012. Distinct cell wall architectures in seed endosperms in representatives of the Brassicaceae and Solanaceae. Plant Physiology **160**, 1551-1566.

Lee Y, Rubio MC, Alassimone J, Geldner N. 2013. A mechanism for localized lignin deposition in the endodermis. Cell **153**, 402-412.

Lee Y, Yoon TH, Lee J, Jeon SY, Lee JH, Lee MK, Chen HZ, Yun J, Oh SY, Wen XH, Cho HK, Mang H, Kwak JM. 2018. A lignin molecular brace controls precision processing of cell walls critical for surface integrity in Arabidopsis. Cell **173**, 1468-1480.

Linkies A, Schuster-Sherpa U, Tintelnot S, Leubner-Metzger G, Müller K. 2010. Peroxidases identified in a subtractive cDNA library approach show tissue-specific transcript abundance and enzyme activity during seed germination of *Lepidium sativum*. J Exp Bot **61**, 491-502.
Narsai R, Law SR, Carrie C, Xu L, Whelan J. 2011. In-depth temporal transcriptome profiling reveals a crucial developmental switch with roles for RNA processing and organelle metabolism that are essential for germination in Arabidopsis. Plant Physiol **157**, 1342-1362.
Nelson BK, Cai X, Nebenfuhr A. 2007. A multicolored set of *in vivo* organelle markers for co-localization studies in *Arabidopsis* and other plants. Plant Journal **51**, 1126-1136.
Pedersen HL, Fangel JU, McCleary B, Ruzanski C, Rydahl MG, Ralet MC, Farkas V, von Schantz L, Marcus SE, Andersen MC, Field R, Ohlin M, Knox JP, Clausen MH, Willats WG. 2012. Versatile high resolution oligosaccharide microarrays for plant glycobiology and cell wall research. J Biol Chem. **287,** 39429-39438.**Raggi S, Ferrarini A, Delledonne M, Dunand C, Ranocha P, De Lorenzo G, Cervone F, Ferrari S**. 2015. The Arabidopsis Class III Peroxidase AtPRX71 Negatively Regulates Growth under Physiological Conditions and in Response to Cell Wall Damage. Plant Physiol **169**, 2513-2525.
Ruprecht C, Bartetzko MP, Senf D, Dallabernadina P, Boos I, Andersen MCF, Kotake T, Knox JP, Hahn MG, Clausen MH, Pfrengle F. 2017. A synthetic glycan microarray enables epitope mapping of plant cell wall glycan-directed antibodies. Plant Physiol **175,** 1094-1104.
Sainsbury F, Thuenemann EC, Lomonossoff GP. 2009. pEAQ: versatile expression vectors for easy and quick transient expression of heterologous proteins in plants. Plant Biotechnol J 7, 682-693.
Saitou N, Nei M. 1987. The neighbor-joining method: a new method for reconstructing phylogenetic trees. Mol Biol Evol **4**, 406-425.
Tognolli M, Penel C, Greppin H, Simon P. 2002. Analysis and expression of the class III peroxidase large gene family in Arabidopsis thaliana. Gene **288**, 129-138.
Xin ZY, Wang AY, Yang GH, Gao P, Zheng ZL. 2009. The Arabidopsis A4 subfamily of Lectin Receptor Kinases negatively regulates abscisic acid response in seed germination. Plant Physiology **149**, 434-444.
Yan JW, He H, Fang L, Zhang A. 2018. Pectin methylesterase31 positively regulates salt stress tolerance in Arabidopsis. Biochemical and Biophysical Research Communications **496**, 497-501.
Zheng BS, Ronnberg E, Viitanen L, Salminen TA, Lundgren K, Moritz T, Edqvist J. 2008. Arabidopsis sterol carrier protein-2 is required for normal development of seeds and seedlings. Journal of Experimental Botany **59**, 3485-3499.
Zimmermann P, Hirsch-Hoffmann M, Hennig L, Gruissem W. 2004. GENEVESTIGATOR. Arabidopsis microarray database and analysis toolbox. Plant Physiol **136**, 2621-2632.

Figure legends

Fig. 1. *Class III Peroxidase* expression data mining allows identifying a micropylar and chalazal endosperm (MCE)-specific *CIII Prx* co-expression cluster. (A) The original gene chip dataset (tissue-specific gene expression of 21,313 protein-coding genes in laser-capture microdissected tissues along *A. thaliana* seed germination kinetics, Dekkers et al., 2013) was retrieved as series matrix files (GSE41212) at https://www.ncbi.nlm.nih.gov/geo/ and edited (**Table S1**). *AtPrx62* (At5g64100) which was the earliest highly expressed *CIII Prx* along the micropylar and chalazal endosperm (MCE) kinetics was used as a bait to calculate the Pearson correlation

coefficient (PCC) for all genes. The genes were subsequently ranked following a decreasing PCC value order. The 23 expressed *CIII Prx* genes present on the microarray are displayed here clearly illustrating a MCE-specific *CIII Prx* co-expression cluster highlighted in blue. A red (max value)-to-yellow (cutoff 5)-to-grey (min value below cutoff) heatmap was drawn for log2 expression values. RAD, radicle; COT, cotyledons; MCE, micropylar and chalazal endosperm; PE, peripheral endosperm; TR, testa rupture; ER, endosperm rupture. The complete data including 37 *AtPrxs* below the cutoff is shown in **Table S2. (B)** Seed germination expression profile of the five candidates (blue text) and their paralogs (red text) showing the germination-specific expression of the candidates. Note that the paralog of *AtPrx62* is also a candidate (*AtPrx71*). Data was retrieved from Genevestigator (Zimmermann *et al.*, 2004) and corresponded to Narsai et al. (2011) (Narsai *et al.*, 2011).

Fig. 2. *AtPrx62, AtPrx69, AtPrx71* and *AtPrx16* transcripts are restricted to the micropylar endosperm of germinating seeds by *in situ* hybridization. Longitudinal sections of 34 hour after sowing (HAS) *A. thaliana* Col germinating seeds were hybridized with antisense (AS, first column) or sense (S, second column) digoxigenin-labeled riboprobes specific for the five *CIII Prxs* selected by co-expression network analysis. The hybridization signals (arrows: purple labeling present on the AS images on the left column and absent in the corresponding S images on the right column) were restricted to the micropylar endosperm and not to the chalazal endosperm for *AtPrx62, AtPrx69, AtPrx71* and *AtPrx16*. No signal could be detected for *AtPrx04*, the least expressed of these five *CIII Prxs* according to transcriptomics (**Table S2**). T: testa (non-specific seed coat natural brown color both in AS and S images); C: cotyledons; R: radicle; PE: peripheral endosperm; CZE: chalazal endosperm; ME: micropylar endosperm; Scale bars: 100 μm. Whole seed views are shown in **Fig. S1.**

Fig. 3. Semi-quantitative comparison of tissue-specific transcriptomics and *in situ* hybridization results. (A) The transcriptomics kinetics data from the micropylar and chalazal endosperm (MCE) was extracted from **Fig. S2** for the five *CIII Prx* candidates showing the sequential initiation of the expression of the five genes. **(B)** Semi-quantitative analysis of *in situ* hybridization (ISH) performed on tissue microarrays at 26, 34, 36 and 38 HAS. For each stage, 10 tissue array serial sections individually hybridized with antisense or sense probes for the five genes were analyzed for expression in micropylar endosperm (ME). Each column represents individual seed serial-section (n = 30 per developmental stage). Color-coding: Red, strong ISH signal in ME; yellow, low ISH signal in ME; white, no ISH signal in ME; black, missing sample. The arrows at

the bottom show seed serial-sections with at least 3 out of the 5 *CIII Prxs* co-expressed. **(C)** Distribution (%) of seed serial-sections displaying ISH signal in ME for 0-to-5 genes along developmental stages. **(D)** The wide view of the tissue array serial-section hybridized with *AtPrx69* AS probe is shown as an example of the method. Individual seed within the white frames have been carefully analyzed at × 20 magnification and color-coded as described above using NDP-view (Hamamatsu).

Fig. 4. AtPrx62, AtPrx69 and AtPrx71 are cell wall localized. Pieces of *Nicotiana benthamiana* leaves transformed with constructs expressing AtPrx62-TagRFP **(A, D-F)**, AtPrx69-TagRFP **(B, G-I)** or AtPrx71-TagRFP **(C, J-L)** either alone **(A-C)** or with constructs expressing PIP2A-YFP used as a plasma membrane (PM) marker **(D-L)** were cut 48 h post-agroinfiltration, and either counterstained with aqueous Calcofluor to label cellulose **(A-C)** or subjected to 30 % glycerol mediated plasmolysis to separate the plasma membrane from the cell wall **(D-L)**. The first line directly shows the merge of the TagRFP fusion proteins as indicated (magenta false color) and calcofluor (green false color) signals. The white signals illustrate the colocalization of AtPrx62-TagRFP **(A)**, AtPrx69-TagRFP **(B)** and AtPrx71-TagRFP **(C)** with the cell wall marker. Under plasmolysis, the fluorescence signal (magenta false color) of AtPrx62-TagRFP **(D-F)**, AtPrx69-TagRFP **(G-I)** and AtPrx71-TagRFP **(J-L)** is excluded from the fluorescence of PIP2A-YFP localized to the plasmolysed plasma membrane (green false color) confirming the cell wall localization of the three TagRFP fusion proteins. CW: cell wall, PM: plasma membrane, Scale bars: 20µm.

Fig. 5. Testa and endosperm ruptures of *Arabidopsis thaliana* seeds are dependent on antagonistic action of several CIII Prxs. (A) Pictures of Col *A. thaliana* seed early germination steps. **(B)** The kinetics of testa rupture (TR, full curves) and endosperm rupture (ER, dashed curves) were monitored for Col, *atprx04-1* and *atprx16-1*. The rates of TR and ER are expressed in % of total number of seeds (± SD) for each time point and for each line. The dashed line corresponds to 50% TR or ER. The time to get 50% of rupture is provided for each line. **(C)** The % of induction or repression of TR at 24 HAS versus Col (± SD) for the ten *CIII Prx* mutants. **(D)** The % of induction or repression of ER at 36 HAS versus Col (± SD) for the ten *CIII Prx* mutants. . The values are the mean of 200 seeds per experiment and they are representative of at least four independent batches of seeds.

Fig. 6. The *AtPrx69* co-expression network is enriched in genes from the "cell wall", "cell wall protein", "xyloglucan" and "germination" tool boxes. Among the co-expression networks of the five *CIII Prx* candidates, *AtPrx69* co-expression network was chosen for this tool box cross-analysis since it showed the most co-expressed pattern of the five *CIII Prxs* **(Table 3)**. Twelve tool boxes gathering lists of genes related to various sub-cellular compartments **(A-D)**, cell wall polymers **(E-H)** and physiological processes **(I-L)** as labeled in the top right corner of each panel, were searched within *AtPrx69* co-expression network built using Dekkers et al (2013) dataset. The x axis corresponds to the Pearson correlation coefficients (PCC) values and the y axis represents the relative rank (%) corresponding for each gene to the ratio of the "tool box rank" hits among *AtPrx69* expression network *vs* the absolute rank within the whole *AtPrx69* expression network. The x axis crosses the y axis at specific thresholds values corresponding to the proportion (%) of the number of expressed genes of each tool box among the 14,317 expressed genes on the microarray (maximum expression value above the "5" cutoff expression value of the transcriptomics). For more details, see **Tables S4 to S15**.

Fig. 7. Complex topochemical diversity of the micropylar endosperm cell wall domains in dry seeds. *A. thaliana* Col dry seed serial longitudinal sections were stained with Toluidine blue (TBO) **(A)** or Calcofluor **(B)** to visualize cell wall morphology and β-glucans, respectively. Serial sections were also immunolabeled with cell wall-specific antibodies and Alexa fluor 488-labeled secondary antibodies. The position of micropylar endosperm (men) is shown with * marks **(C-R)**. Negative controls without primary antibodies were also performed **(S-T)**. The antibodies are noted on the top right corner of the images and classified using background color codes. The green lines/spots around the simplified drawing displayed on the right of each image summarize the observed immunofluorescence patterns within a men cell. The absence of green line with some antibodies corresponds to the absence of labeling as compared to the negative controls (See Table S17 and methods for a complete list of the antibodies tested). The non specific autofluorescence allowing to visualize the morphology is displayed in magenta false color. The Alexa-488 specific signal is visualized in bright green. Note that the confocal microscopy settings were adjusted to visualize either intense and fainter A488 signals depending on the antibodies. The greenish autofluorescence labels correspond to fainter signals. The negative control without primary antibodies is displayed using both settings. pd, radicle protodermis; men (*), micropylar endosperm; ii1, inner integument 1 cell layer; oi2, outer integument 2 cell layer. Bars: 25 µm.

Fig. 8. Integrated model of spatiotemporal coordinated roles of functionally redundant and non-redundant ME CW-remodeling or ME CW integrity-sensing proteins from four multigenic families. (A) The tissue-specific germination transcriptomics data (Dekkers *et al.*, 2013) was used to assemble MCE-specific expression values for the five *CIII Prxs* and to integrate those with corresponding values from previously characterized additional ME CW-remodeling enzymes: 3 Mananases (MAN) (Iglesias-Fernandez *et al.*, 2011) and 2 xyloglucan xylosyltransferases (XXT) (Lee *et al.*, 2012), and putative ME CW integrity sensors: 3 Lectin Receptor kinases (LecRK) (Xin *et al.*, 2009). Comparison of phenotypes and expression profiles indicated that the genes having slightly sequential expression had non redundant functions since simple mutant displayed germination phenotypes (3 MANs and 5 CIII-Prxs) while those having more highly co-expression profiles had redundant functions requiring multiple mutants to see the germination phenotypes (3 LecRKs and 2 XXTs). The ME CW loosening (green label) or stiffening (red lab) roles were deducted from the delayed and accelerated germination phenotypes, respectively. **(B)** Spatio-temporal integrated model of ME CW fine remodeling necessary to control germination. The drawings show a zoom on the interface between the growing radicle (Rad), the micropylar endosperm (ME) and the testa at various times expressed as hours after sowing. The timing of apparition of individual ME CW remodeling proteins follows transcriptomics. The growing-radicle increasing pressure (large green arrow) is first accompanied by the ME CW sequential loosening role of 3 MANS (green label), which in turn is counterbalanced by the ME CW sequential stiffening role of 4 CIII Prxs (red label) and finally accompanied by the ME CW loosening role of AtPrx04 (green label). The additional ME CW redundant loosening role of the two constitutive XXTs and the 3 late expressed LecRKs was not displayed for clarity. Altogether, the phenotypes observed in each *man* and *CIII prx* mutants, indicating their non-redundant roles, could be explained by their subtle sequential apparition and/or by putative yet-to-be demonstrated ME microdomain localization.

Fig. 1

A

Absolute PCC Rank	*AtPrx62* expression network (PCC)	Annotation	AGI number	Dry Seed	1h	3h	7h	12h	16h	20h	25h noTR	25h TR	31h	38h noER	38h ER	3h	16h	31h	1h	3h	7h	12h	16h	20h	25h noTR	25h TR	31h	38h noER	38h ER	3h	16h	31h
					Seed RAD											Seed COT			Seed MCE											Seed PE		
1	1.00000	*AtPrx62*	At5g39580	3	3	3	3	4	3	3	3	4	4	4	6	4	4	5	4	6	9	7	10	9	9	13	13	12	13	5	9	12
155	0.88882	*AtPrx69*	At5g64100	4	4	4	4	4	4	3	4	4	4	5	9	4	3	3	4	4	3	4	9	9	9	12	13	13	13	4	5	9
457	0.81544	*AtPrx71*	At5g64120	3	3	3	3	3	3	3	3	3	3	3	4	3	3	4	3	3	3	3	5	5	5	9	9	10	12	3	3	6
940	0.74235	*AtPrx16*	At2g18980	4	4	4	4	4	4	4	4	4	4	5	8	4	4	4	4	4	4	4	4	4	6	9	11	11	11	4	4	9
953	0.73961	*AtPrx04*	At1g14540	3	3	3	3	3	3	3	3	4	3	3	4	3	3	4	3	3	3	3	3	3	4	7	6	9	10	3	3	5
1121	0.71487	*AtPrx52*	At5g05340	3	4	3	3	3	3	3	3	3	3	3	3	3	3	3	3	3	3	4	3	3	3	4	5	5	5	3	3	3
1467	0.66515	*AtPrx12*	At1g71695	8	3	3	3	3	3	3	3	3	3	6	7	7	5	7	9	9	8	7	8	8	8	8	9	9	9	9	8	8
1823	0.61700	*AtPrx30*	At3g21770	4	4	4	4	3	4	4	4	4	3	4	4	4	4	4	4	4	3	3	4	4	5	5	6	4	4	4	4	8
2770	0.49640	*AtPrx05*	At1g14550	3	3	3	3	3	3	3	3	3	3	3	4	3	3	3	4	3	3	3	3	3	3	4	3	5	7	3	4	3
3032	0.46925	*AtPrx70*	At5g64110	3	3	3	3	3	3	3	3	3	3	3	3	3	3	3	3	3	3	3	3	3	3	3	3	6	7	3	3	3
4251	0.31703	*AtPrx57*	At5g17820	3	3	3	3	3	3	3	3	3	3	3	7	3	3	3	3	3	3	3	3	3	3	3	3	6	7	3	3	3
4557	0.27395	*AtPrx45*	At4g30170	3	3	3	3	3	3	3	3	3	5	8	3	3	3	3	3	3	3	3	3	3	3	3	3	6	7	3	3	3
5463	0.15029	*AtPrx17*	At2g22420	3	3	3	6	9	9	8	8	8	6	6	5	3	9	8	3	3	4	8	9	8	8	7	7	5	4	3	9	7
5586	0.13362	*AtPrx31*	At3g28200	5	5	6	7	8	8	8	8	8	8	8	9	6	7	7	4	5	6	7	7	7	7	9	8	7	7	5	7	6
7374	-0.09222	*AtPrx66*	At5g51890	4	4	4	4	3	3	3	3	3	3	4	5	3	3	4	4	3	3	3	3	3	3	3	3	3	4	3	3	3
7452	-0.10086	*AtPrx27*	At3g01190	3	3	3	3	3	3	3	3	3	3	4	7	3	3	3	3	3	3	3	3	3	3	3	3	3	3	3	3	3
7584	-0.11542	*AtPrx07*	At1g30870	4	4	4	4	4	4	4	4	4	4	4	7	4	4	4	4	4	4	4	4	4	4	4	4	4	4	4	4	4
8079	-0.16899	*AtPrx46*	At4g31760	3	3	3	3	3	4	4	4	5	5	5	5	3	4	7	3	3	3	3	3	3	4	4	4	4	4	3	3	4
9762	-0.34043	*AtPrx37*	At4g08770	3	3	3	3	3	3	4	5	5	5	5	6	3	3	3	3	3	3	3	3	3	3	3	3	3	3	3	3	3
10374	-0.39535	*AtPrx19*	At2g34060	4	4	4	4	4	4	4	4	4	4	5	5	4	4	4	4	4	4	4	4	4	4	4	4	4	4	4	4	4
10509	-0.40762	*AtPrx26*	At2g43480	3	3	3	3	3	4	5	6	6	7	6	6	3	3	3	3	3	3	3	3	3	3	3	3	3	3	3	3	3
11061	-0.45499	*AtPrx63*	At5g40150	3	3	4	4	5	6	6	6	6	6	6	5	3	5	6	3	3	3	3	4	4	4	4	3	4	4	3	4	4
13585	-0.72629	*AtPrx42*	At4g21960	7	8	8	8	10	10	10	11	11	10	11	10	6	7	6	7	7	6	7	6	6	5	5	4	5	5	6	6	4

B

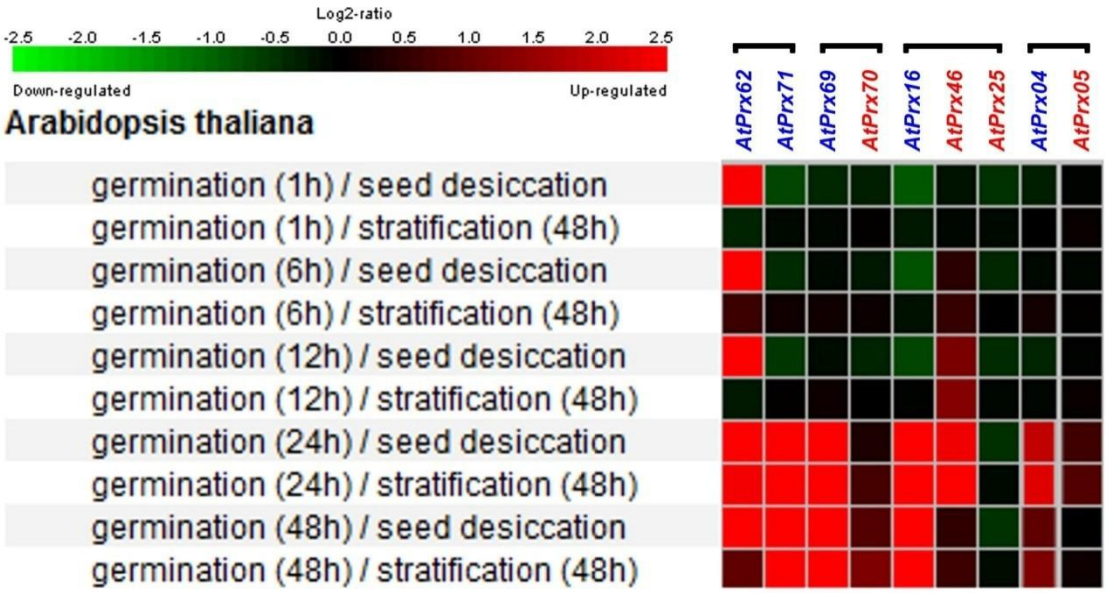

Fig. 2

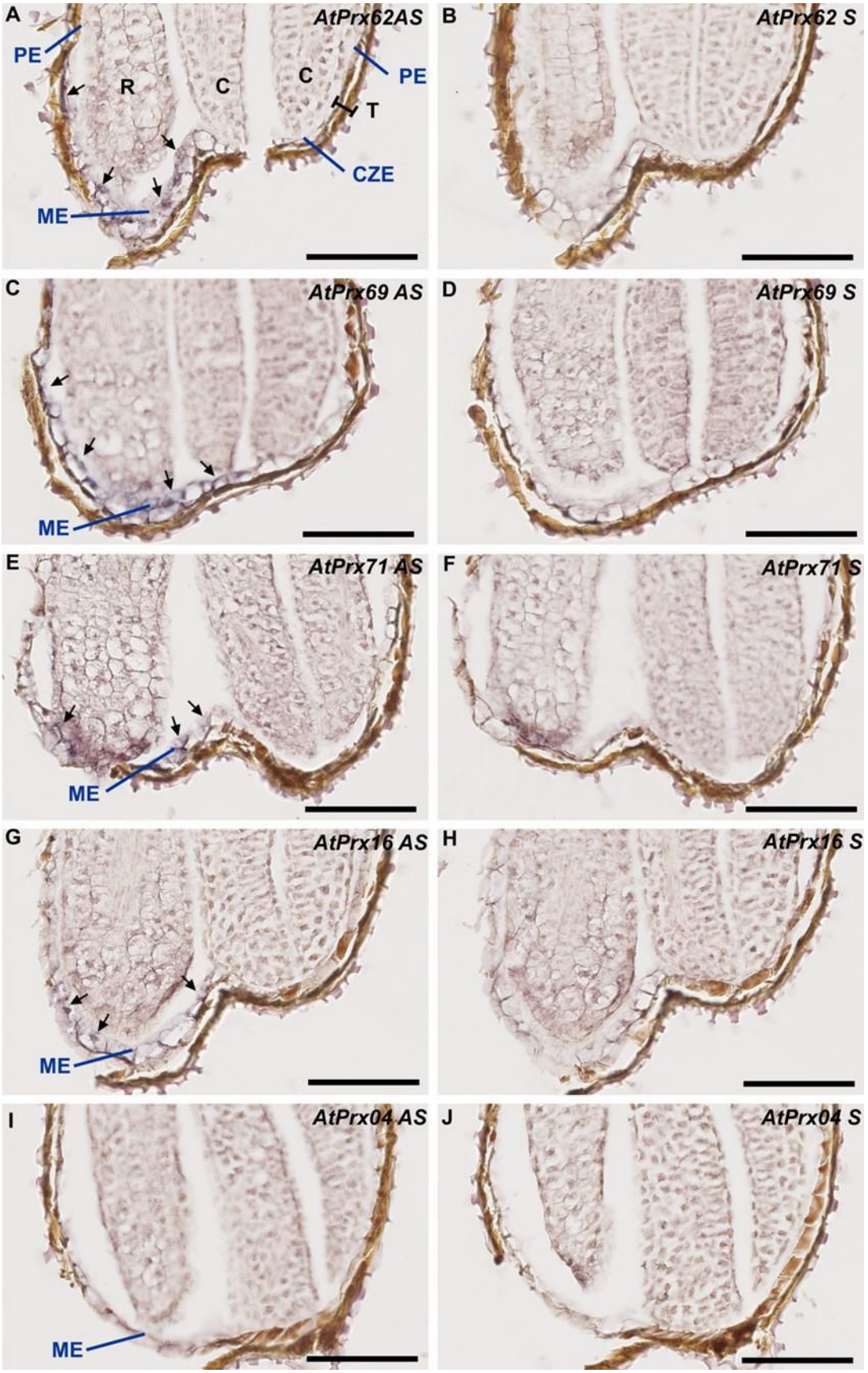
A
AtPrx62AS
PE
R
C
C
PE
T
CZE
ME
B
AtPrx62 S
C
AtPrx69 AS
ME
D
AtPrx69 S
E
AtPrx71 AS
ME
F
AtPrx71 S
G
AtPrx16 AS
ME
H
AtPrx16 S
I
AtPrx04 AS
ME
J
AtPrx04 S

Fig. 3

A

Annotation	AGI number	Maximum Expression Value Rank	Maximum Expression value	1h	3h	7h	12h	16h	20h	25h noTR	25h TR	31h	38h noER	38h ER
				Seed MCE										
AtPrx62	At5g39580	212	13.0	3.6	6.0	8.6	6.5	10.3	8.8	9.3	12.6	13.0	12.3	12.7
AtPrx69	At5g64100	99	13.5	3.8	3.6	3.5	3.9	8.9	9.2	9.3	12.1	13.1	13.4	13.5
AtPrx71	At5g64120	681	11.8	3.4	3.3	3.3	3.4	4.7	4.6	4.5	8.6	8.8	10.4	11.8
AtPrx16	At2g18980	1019	11.3	3.7	3.9	3.7	3.8	3.8	4.3	5.8	9.0	11.3	11.2	10.9
AtPrx04	At1g14540	2136	10.4	3.1	2.8	3.0	3.1	3.4	3.3	4.3	6.6	5.9	9.2	10.4

B

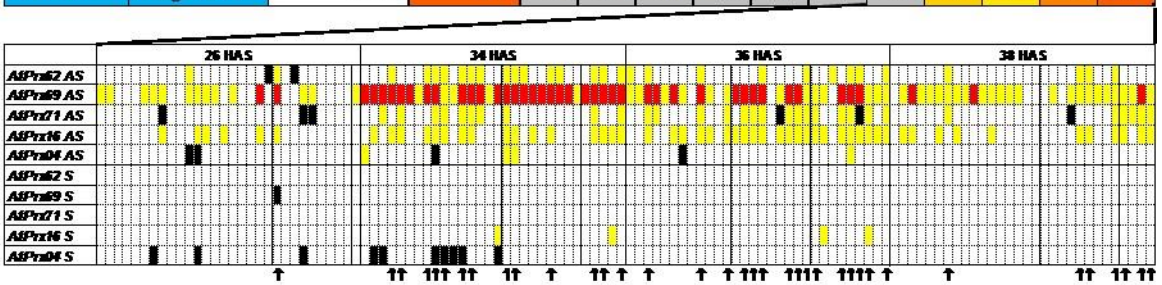

C

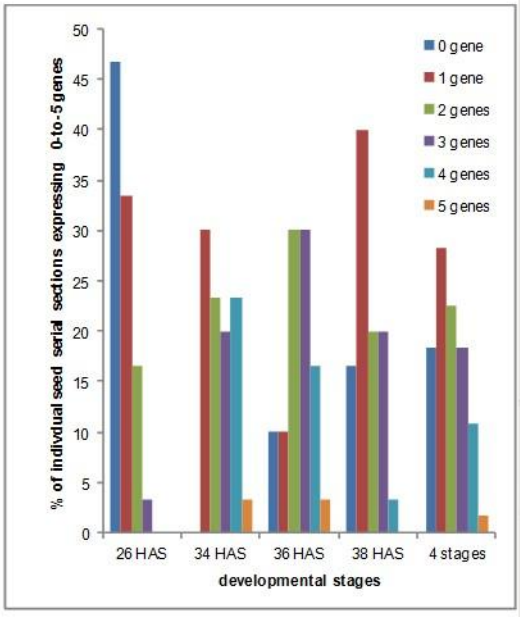

D

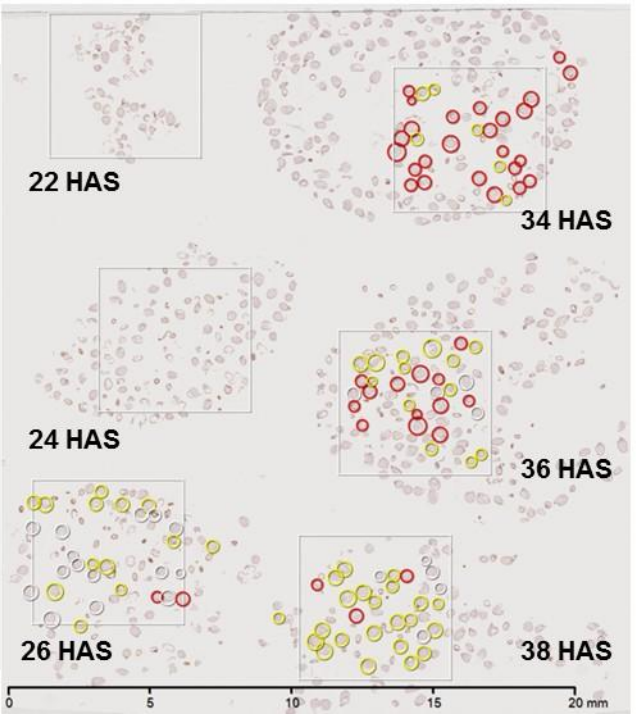

Fig. 4

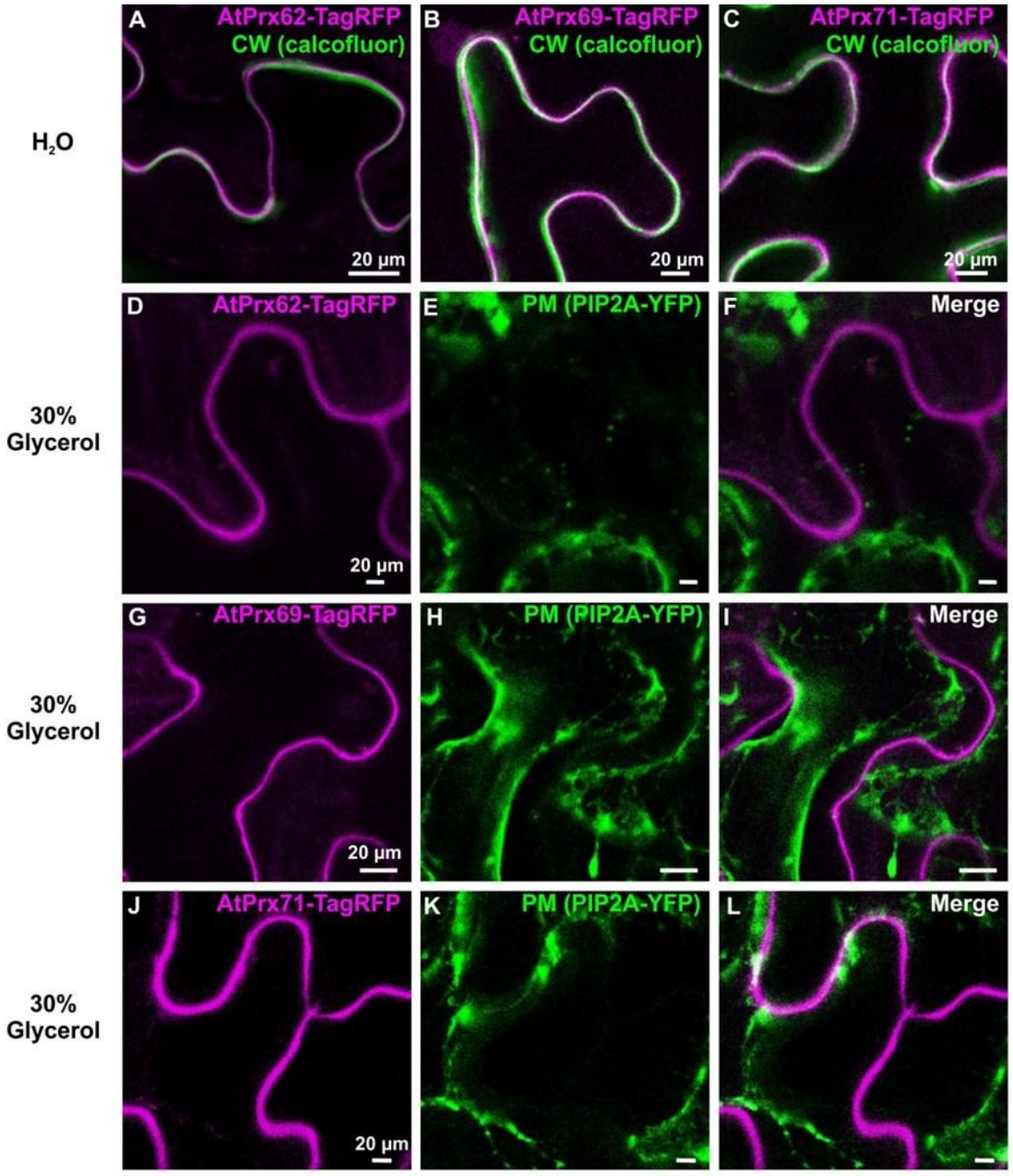
H2O
30% Glycerol
30% Glycerol
30% Glycerol
A
AtPrx62-TagRFP
CW (calcofluor)
20 µm
B
AtPrx69-TagRFP
CW (calcofluor)
20 µm
C
AtPrx71-TagRFP
CW (calcofluor)
20 µm
D
AtPrx62-TagRFP
20 µm
E
PM (PIP2A-YFP)
F
Merge
G
AtPrx69-TagRFP
20 µm
H
PM (PIP2A-YFP)
I
Merge
J
AtPrx71-TagRFP
20 µm
K
PM (PIP2A-YFP)
L
Merge

Fig. 5

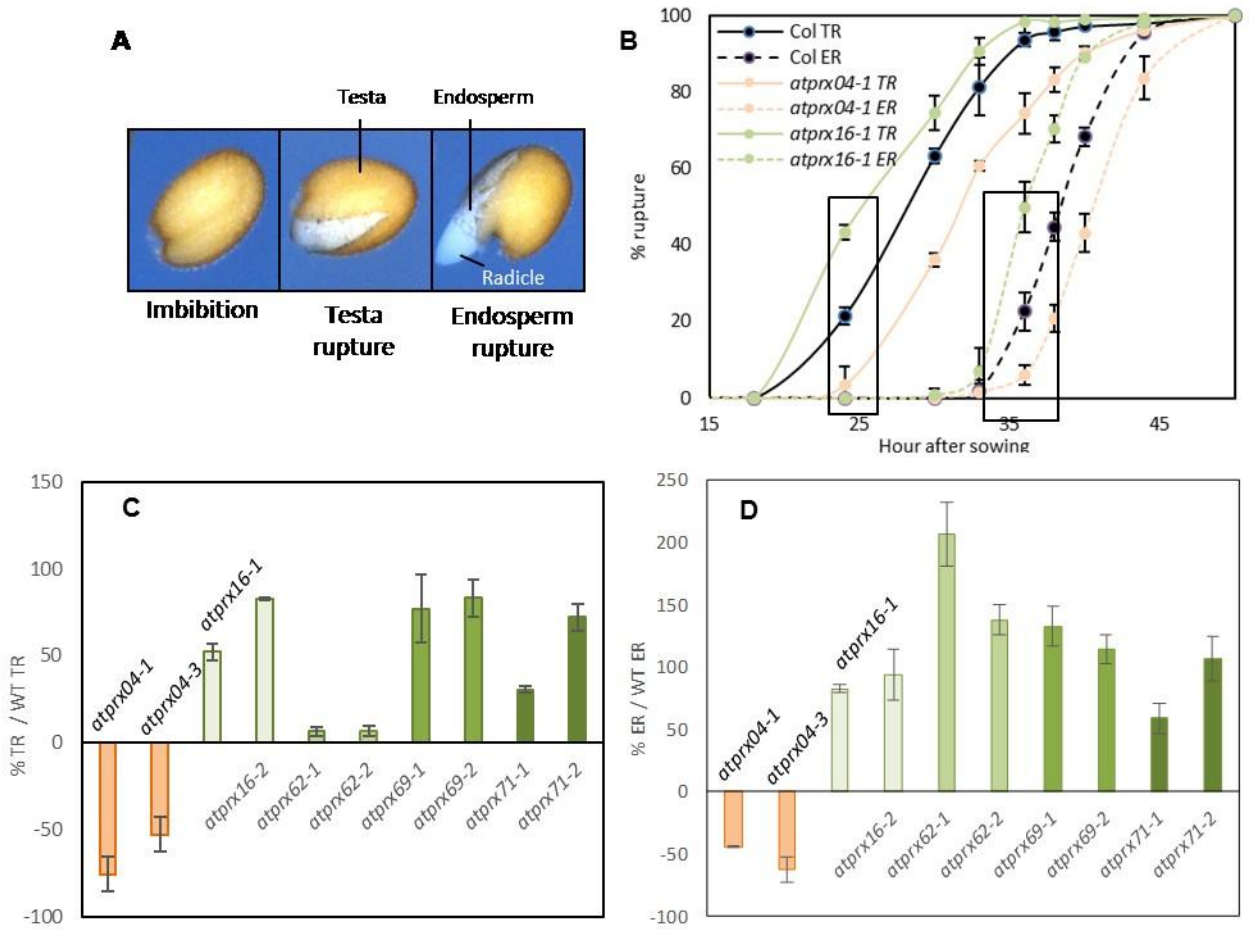
A
Testa
Endosperm
Radicle
Imbibition
Testa rupture
Endosperm rupture
B
Col TR
Col ER
atprx04-1 TR
atprx04-1 ER
atprx16-1 TR
atprx16-1 ER
% rupture
Hour after sowing
C
% TR / WT TR
atprx04-1
atprx04-3
atprx16-1
atprx16-2
atprx62-1
atprx62-2
atprx69-1
atprx69-2
atprx71-1
atprx71-2
D
% ER / WT ER
atprx04-1
atprx04-3
atprx16-1
atprx16-2
atprx62-1
atprx62-2
atprx69-1
atprx69-2
atprx71-1
atprx71-2

Fig. 6

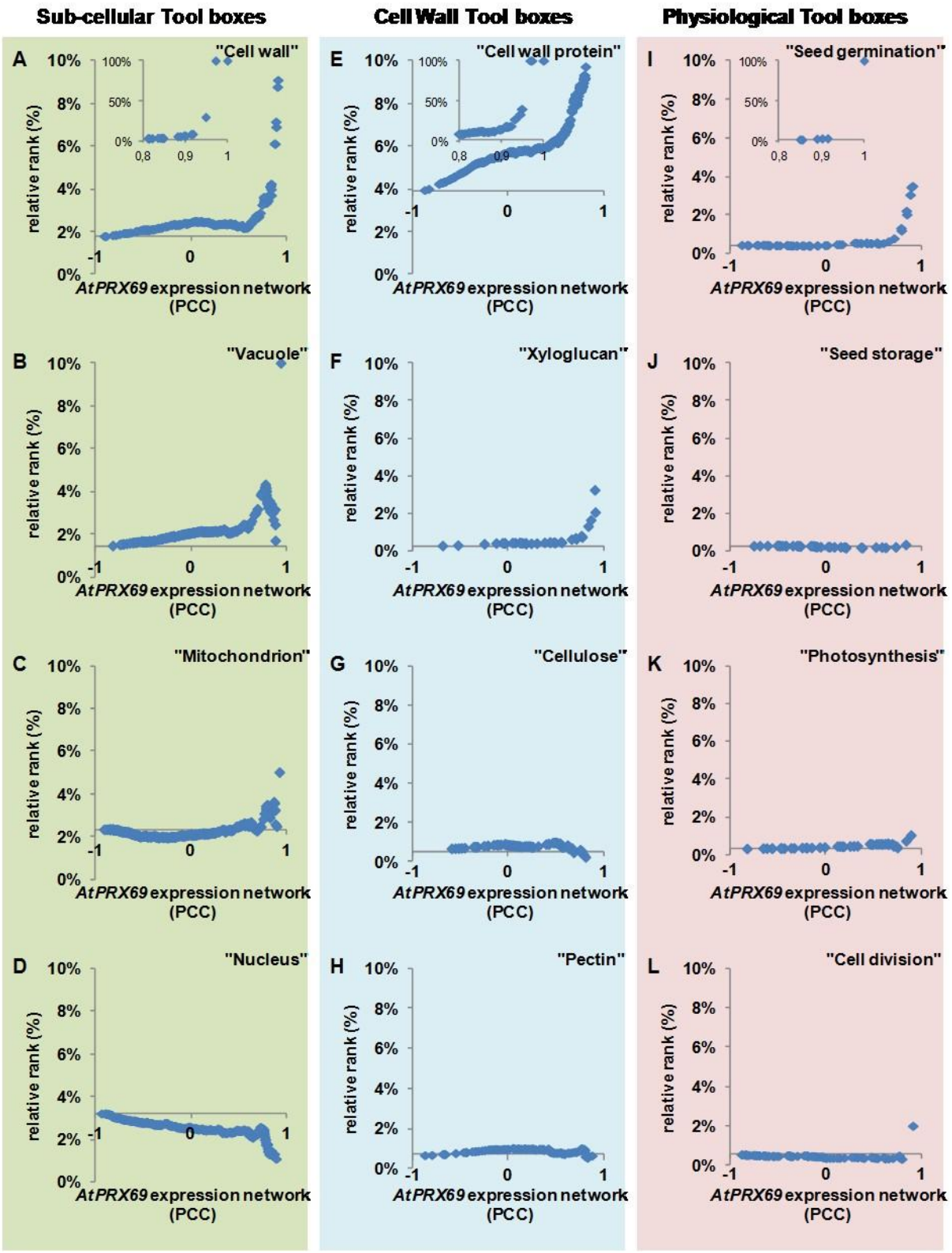
Sub-cellular Tool boxes
Cell Wall Tool boxes
Physiological Tool boxes
A
"Cell wall"
B
"Vacuole"
C
"Mitochondrion"
D
"Nucleus"
E
"Cell wall protein"
F
"Xyloglucan"
G
"Cellulose"
H
"Pectin"
I
"Seed germination"
J
"Seed storage"
K
"Photosynthesis"
L
"Cell division"
relative rank (%)
AtPRX69 expression network (PCC)

Fig. 7

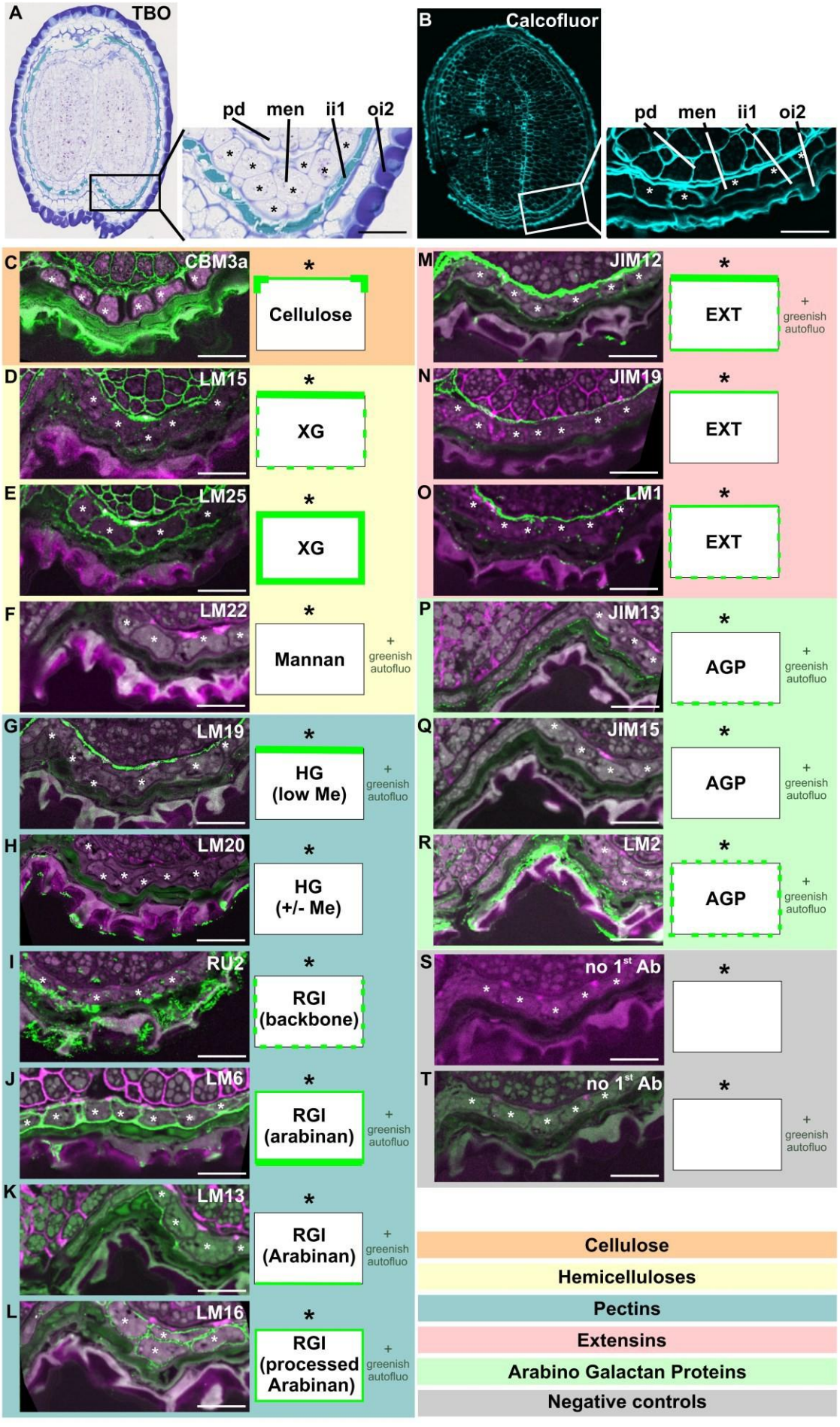
A
TBO
pd
men
ii1
oi2
B
Calcofluor
pd
men
ii1
oi2
C
CBM3a
*
Cellulose
D
LM15
*
XG
E
LM25
*
XG
F
LM22
*
Mannan
+ greenish autofluo
G
LM19
*
HG (low Me)
+ greenish autofluo
H
LM20
*
HG (+/- Me)
I
RU2
*
RGI (backbone)
J
LM6
*
RGI (arabinan)
+ greenish autofluo
K
LM13
*
RGI (Arabinan)
+ greenish autofluo
L
LM16
*
RGI (processed Arabinan)
+ greenish autofluo
M
JIM12
*
EXT
+ greenish autofluo
N
JIM19
*
EXT
O
LM1
*
EXT
P
JIM13
*
AGP
+ greenish autofluo
Q
JIM15
*
AGP
+ greenish autofluo
R
LM2
*
AGP
+ greenish autofluo
S
no 1st Ab
*
T
no 1st Ab
*
+ greenish autofluo
Cellulose
Hemicelluloses
Pectins
Extensins
Arabino Galactan Proteins
Negative controls

Fig. 8

A

Functional redundancy	AGI number	Annotation	1h	3h	7h	12h	16h	20h	25h noT R	25h TR	31h	38h noE R	38h ER	Germination phenotype	Deducted ME CW remodeling role
			Seed MCE												
Non Redundant	AT4g28320	AtMAN5	5.0	5.6	4.6	3.9	3.8	3.6	3.7	3.6	3.6	3.5	3.0	Delayed	Loosening
Non Redundant	AT5g01930	AtMAN6	5.7	6.8	5.7	4.5	4.3	4.1	4.0	4.0	3.9	3.9	4.0	Delayed	Loosening
Non Redundant	AT5g66460	AtMAN7	6.3	5.8	6.5	10.3	11.4	11.6	11.6	10.9	9.3	6.9	5.4	Delayed	Loosening
Non Redundant	AT5g39580	AtPrx62	3.6	6.0	8.6	6.5	10.3	8.8	9.3	12.6	13.0	12.3	12.7	Accelerated	Stiffening
Non Redundant	AT5g64100	AtPrx69	3.8	3.6	3.5	3.9	8.9	9.2	9.3	12.1	13.1	13.4	13.5	Accelerated	Stiffening
Non Redundant	AT2g18980	AtPrx16	3.7	3.9	3.7	3.8	3.8	4.3	5.8	9.0	11.3	11.2	10.9	Accelerated	Stiffening
Non Redundant	AT5g64120	AtPrx71	3.4	3.3	3.3	3.4	4.7	4.6	4.5	8.6	8.8	10.4	11.8	Accelerated	Stiffening
Non Redundant	AT1g14540	AtPrx04	3.1	2.8	3.0	3.1	3.4	3.3	4.3	6.6	5.9	9.2	10.4	Delayed	Losening
Redundant	AT5g01550	AtLecRKA4.2	3.8	3.6	3.5	3.5	3.5	3.3	3.4	3.6	3.8	5.2	6.8	Delayed	Loosening
	AT5g01560	AtLecRKA4.3	3.1	3.3	3.1	3.2	3.1	3.1	3.1	3.1	3.1	4.2	5.3		
	AT5g01540	AtLecRKA4.1	3.2	3.3	3.4	3.5	3.4	3.5	3.5	3.8	3.7	4.9	6.1		
Redundant	AT3g62720	AtXXT1	6.9	8.5	7.8	7.9	9.8	8.8	8.9	9.9	9.0	8.9	8.8	Delayed	Loosening
	AT4g02500	AtXXT2	8.5	8.2	7.5	6.5	6.7	7.6	7.9	8.4	8.1	7.4	7.3		

B